GDCh

Research Article

Angewandte
International Edition
Chemie
www.angewandte.org

Check for updates

VIP *AI for Materials* *Very Important Paper*

Unraveling the Complexity of Divalent Hydride Electrolytes in Solid-State Batteries via a Data-Driven Framework with Large Language Model

Qian Wang, Fangling Yang, Yuhang Wang, Di Zhang, Ryuhei Sato, Linda Zhang, Eric Jianfeng Cheng, Yigang Yan, Yungui Chen, Kazuaki Kisu, Shin-ichi Orimo, and Hao Li*

Abstract: Solid-state electrolytes (SSEs) are essential for next-generation energy storage technologies. However, the exploration of divalent hydrides is hindered by complex ionic migration mechanisms and reliance on "trial-and-error" methodologies. Conventional approaches, which focus on individual materials and predefined pathways, remain inefficient. Herein, we present a data-driven artificial intelligence framework that integrates a comprehensive SSE database with large language models and ab initio metadynamics (MetaD) simulations to accelerate the discovery of hydride SSEs. Our study reveals that hydrides incorporating neutral molecules have great potential, with MetaD revealing novel "two-step" ion migration mechanisms. Predictive models developed using both experimental and computational data accurately forecast ionic migration activation energies for various types of hydride SSEs. In particular, some SSEs with carbon-containing neutral molecules exhibit notably low activation energy, with barriers as low as 0.62 eV. This framework enables the rapid identification of optimized SSE candidates and establishes a transformative tool for advancing sustainable energy storage technologies.

Introduction

The development of next-generation energy materials is crucial for a sustainable future, with batteries playing a key role in powering electric vehicles, electronics, and energy systems. Solid-state batteries (SSBs) offer a promising solution, yet their development presents significant technical challenges. Companies like Toyota, which holds over 1000 patents in this field, and institutions like the U.S. Department of Energy (DOE) have set ambitious targets for improving the solid-state electrolyte (SSE) performance for SSB development.[1] These goals include enhancing ionic conductivity, stability, and cycle life to extend the range of electric vehicles to 1000 miles and reduce charging times to less than 10 min.[1] However, achieving these targets remains difficult due to the limitations of current materials.

To address these challenges, the development of high-performance SSE materials is essential for unlocking the full potential of SSBs. Batteries with higher specific energy, improved safety, and longer service life are critical to meet the demands of large-scale energy storage and diverse electronics.[2] Among these, all-solid-state batteries (ASSBs) are receiving intense research attention due to their ability to enhance both energy density and safety.[3,4] While metal oxides and sulfides have been widely studied as promising SSEs,[5,6] the exploration of hydrides as SSEs that exhibit high redox and mechanical stability and moderate divalent ionic conductivity at room temperature is becoming increasingly urgent.[7,8]

Metal hydrides offer unique advantages due to the light mass of hydrogen atoms in boranes such as $[BH_4]^-$ and $[B_{12}H_{12}]^{2-}$, which facilitate ion transfer through mechanisms

[*] Q. Wang, F. Yang, Y. Wang, D. Zhang, L. Zhang, E. J. Cheng, S.-ichi Orimo, H. Li
Advanced Institute for Materials Research (WPI-AIMR), Tohoku University, Sendai 980–8577, Japan
E-mail: li.hao.b8@tohoku.ac.jp

Q. Wang, Y. Yan, Y. Chen
Institute of New Energy and Low-Carbon Technology, Sichuan University, Chengdu 610207, China

R. Sato
Department of Materials Engineering, The University of Tokyo, 7-3-1 Hongo Bunkyo-ku, Tokyo 113–8656, Japan

Y. Yan, Y. Chen
Engineering Research Center of Alternative Energy Materials and Devices, Ministry of Education, China

K. Kisu
College of Engineering, Shibaura Institute of Technology, Tokyo 135–8548, Japan

S.-ichi Orimo
Institute for Materials Research (IMR), Tohoku University, Sendai 980–8577, Japan

Additional supporting information can be found online in the Supporting Information section

like the paddle-wheel mechanism.[9–11] Hydrides have shown great promise in SSE development, with high ionic conductivity ($\sim 1 \times 10^{-3}$ S cm^{-1} at room temperature) and low activation energy (E_a).[12,13] Boranes are classified into three types: *closo*-boranes (e.g., $B_nH_n^{2-}$), which are closed polyhedral (cage-like) clusters, *nido*-boranes (e.g., $B_nH_{n+3}^{-}$), and *arachno*-boranes (e.g., $B_nH_{n+5}^{-}$).[14] For instance, the most well-known *nido*-boranes, LiBH$_4$, has shown high ionic conductivity, especially after undergoing a high-temperature phase transition (2×10^{-3} S cm^{-1} at >400 K).[15] Recent research has also expanded into exploring alternative systems based on abundant elements such as Mg(BH$_4$)$_2$ and Ca(BH$_4$)$_2$, both of which offer higher energy densities.[16] However, the presence of divalent cations in these materials intensifies electrostatic interactions, hindering ionic migration and complicating experimental investigations.[17,18] One approach to address this issue involves introducing neutral molecules like NH$_3$, which form double hydrogen bonds with [BH$_4$] $^{-}$, thereby reducing coordination strength and facilitating Mg ion migration.[19] Despite this, the light weight of hydrogen and the complex behavior of divalent hydrides present additional challenges in batch synthesis and structural characterization, highlighting the limitations of current experimental techniques. Currently, experimental SSE discovery mainly relies on inefficient, time-consuming trial-and-error methods.

To meet this challenge, computation-assisted research plays an increasingly critical role in understanding ionic migration mechanisms and discovering novel SSEs. Computational strategies such as molecular dynamics (MD), ab initio MD (AIMD),[20,21] bond valence site energy (BVSE),[22] climbing-image nudged elastic band (CI-NEB),[23,24] and machine learning force field-based MD (MLMD) provide atomistic insights into energy barriers and migration mechanisms.[25] These techniques allow researchers to investigate various processes in SSEs, such as cation migration kinetics and activation energy barriers, across different spatial and temporal scales.[26] In contrast to experimental methods, which often rely on trial and error, theoretical approaches offer a faster and more systematic way to explore material properties. Recent advancements in large language models (LLMs) have further enhanced data-driven methodologies, facilitating broader accessibility for chemists and potentially improving theoretical predictions.[27] Nevertheless, due to the complexity of SSE materials, achieving a high accuracy in theoretical methods remains challenging. Moreover, current research frequently focuses on a single method or material, limiting the comprehensive understanding of SSEs. All these challenges can be summarized by the following critical questions:

> *How can theoretical insights be better leveraged to design more efficient experiments, and what would an optimal workflow look like that seamlessly combines theoretical modeling with experimental validation?*

To overcome the limitations of divalent SSEs, including *closo-*, *nido*-, and *arachdo*-type hydrides, which show significant promise for high-performance ASSBs, herein, we developed an integrated workflow combining data mining, artificial intelligence (AI)-driven analysis, ab initio meta-

dynamics (MetaD) simulations, theory-experiment benchmarking, machine learning regression, and global structure search. This approach aims to unravel the intricate structure-performance relationships of SSEs. By bridging theory and experiments, we aim to understand the complex structure-performance relationships of SSEs. This integrated approach allows us to establish accurate predictive models for activation energies (E_a), identify stable crystal structures, and reduce reliance on extensive experimental data. Our work not only enhances the understanding of divalent SSEs but also provides a robust framework to predict and design new SSE candidates, facilitating the efficient discovery and optimization of materials for next-generation energy storage technology.

Results and Discussion

Data-Driven and AI-Accelerated Workflow to Understand High-Performance SSEs

Despite the combined efforts of experimental and computational studies, the limitations of divalent SSEs remain elusive, largely due to the constraints of current materials characterization techniques and simulation methods. The variability of neutral molecules and sluggish ionic migration further complicate the investigation of these systems. To overcome these challenges, herein, we have developed an innovative, big data-driven workflow combining large language models (LLM) to better understand SSEs and analyze cation migration, aiming to design fast ion-conducting SSEs for high-performance SSBs (Figure 1a). This workflow starts with big data analysis, utilizing our recently developed database (i.e., the Dynamic Database of Solid-State Electrolyte (DDSE),[28] which contains **2556** experimental SSE materials, **18635** sets of ion conductivity measurements and **657** computational SSE materials) to capture and establish key features. Leveraging this comprehensive database, an LLM is employed to rapidly enhance our understanding of advanced SSEs, resulting in two significant insights detailed in the following sections. A visual demonstration of how these insights were generated by the LLM is provided in the Supporting Video.

LLM Insight 1: Hydride SSEs with Neutral Molecules

While a single literature report is generally limited to insights into one or several SSE materials, big data analysis paves a new avenue to comprehensively and fairly overview the development of SSEs across various types of materials and the key variables. Based on insights derived from the LLM (as illustrated in the Supporting Video), Figure 1b summarizes the temperature-dependent ionic conductivity of **158** metal hydrides, as reported in experimental studies available to date. For the SSEs without neutral molecules, monovalent electrolytes exhibit conductivity ranging from 10^{-7} to 10^{-1} S cm^{-1} coupled with a low E_a of <1.0 eV. However, with the same type of anion, divalent ions are less likely to conduct at the same temperature likely due to their stronger
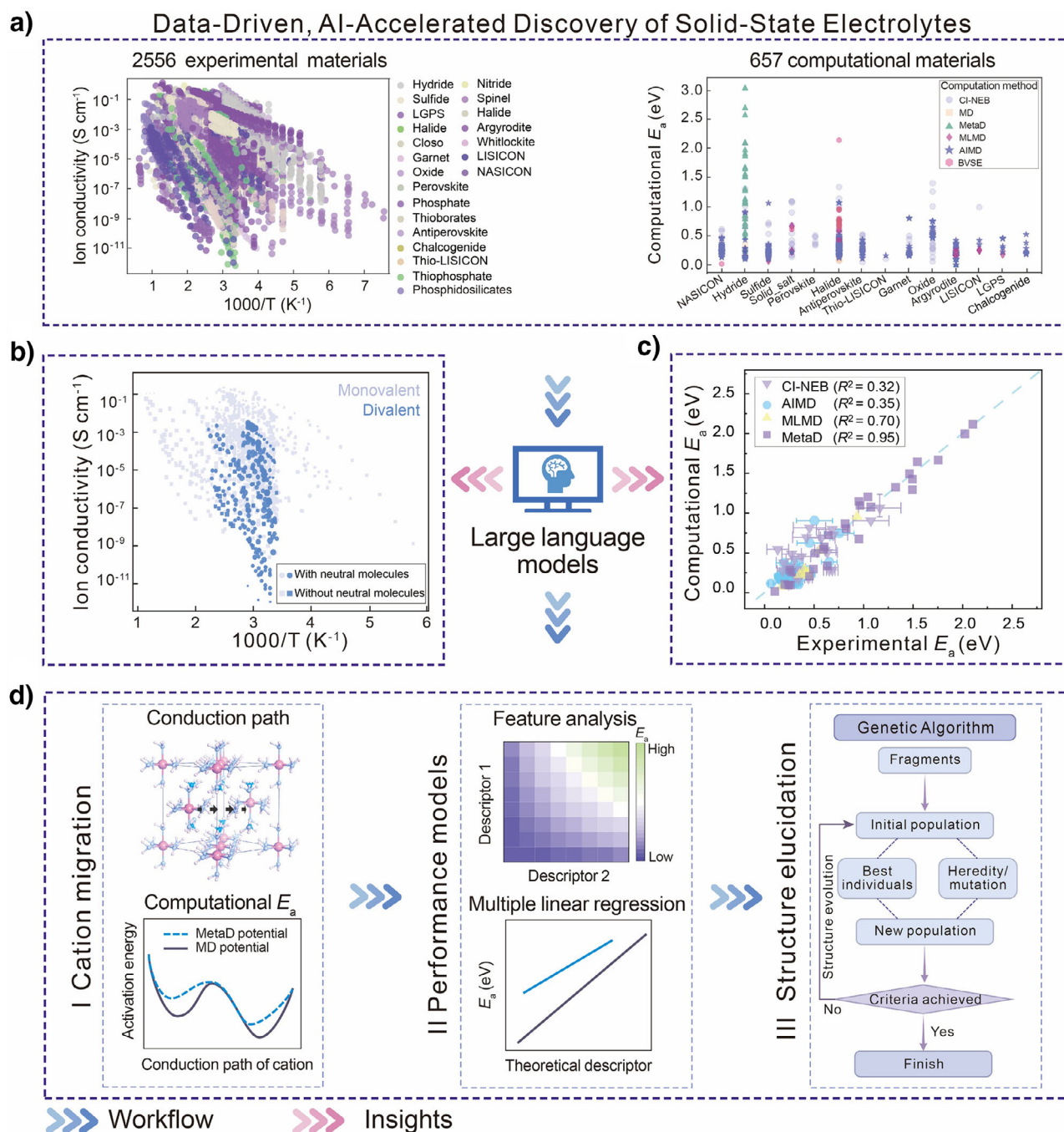
Figure 1. Big data-driven AI analysis of hydride SSEs. a) Left: Temperature profiles of the ionic conductivity of all types SSEs extracted from available experimental data reported to date. Right: Computational E_a values obtained using different methods for all types SSEs reported to date. b) Temperature profiles of the ionic conductivity of hydride SSEs extracted from available experiments reported to date. Point size represents the E_a value, with larger points indicating higher E_a. c) Benchmarking analysis between experimental E_a and the computational E_a from different methods. All the data sources are available in the DDSE database. Detailed introduction and insights regarding the LLM are provided in the Supporting Video. d) Schematic diagram of the proposed workflow to develop high-performance SSEs.

electrostatic interactions. As a result, divalent SSEs without neutral molecules are rare. Notably, the addition of neutral molecules to the divalent SSE lattice promotes divalent ion migration, significantly increasing both the conductivity and the availability of divalent SSEs. Their performance even rivals that of monovalent electrolytes, with ionic conductiv-

ities exceeding 1.5×10^{-4} S cm^{-1} at 303 K.[29] Similarly, monovalent electrolytes also exhibit a dramatic increase in conductivity with the addition of neutral molecules, e.g., the ionic conductivity of LiBH$_4$ increases from 8×10^{-8} to 7×10^{-4} S cm^{-1} when complexed with NH$_3$ at 313 K (LiBH$_4$·1/2NH$_3$).[30]

LLM Insight 2: Significant Discrepancy Between Conventional Simulations and Experiments

To understand ionic migration in these SSE materials, cost-effective predictions of ionic transport are crucial to guide SSEs design. During the past decade, some computational approaches, including static DFT computations and AIMD simulations, have been employed to analyze ionic migration mechanisms of SSEs.[31,32] Building on the insight derived from LLM (as illustrated in the Supporting Video), Figure 1c provides a comparison between the experimental and computational E_a for various SSE materials, demonstrating the accuracy of different computational methods. Surprisingly, most previous reports with conventional simulation methods prioritize trend comparisons, sometimes leading to large deviations from experimental results. For instance, CI-NEB can only capture one transition state once the initial pathway is artificially tailored, which may lead to significant discrepancies between the calculated and experimental E_a, even resulting in an R^2 value of 0.32. One typical example is the use of CI-NEB to compute the E_a of Li^+ in γ-Li_3PS_4 and obtained a value of 0.7 eV,[33] compared to the experimental value of 0.22 eV or 0.49 eV showing a discrepancy of 0.48 and 0.21 eV,[34,35] respectively. AIMD, which simulates ionic conductivity at high temperatures and extrapolates to lower temperatures by determining E_a, provides another option to sample the reaction paths. For instance, while CI-NEB estimated the E_a for LiTaSiO$_5$ as 0.82 eV, AIMD simulations yielded an E_a of 0.63 eV, much closer to the experimental value (0.46 eV).[36] Unfortunately, AIMD still generally shows a significant deviation ($R^2 = 0.35$) and is limited by high computational cost, restricting it to small lattice sizes and short simulation timescales. Machine learning (ML) force fields enable efficient MD simulations, but MLMD still faces significant discrepancies ($R^2 = 0.70$) and challenges with both sampling and force field accuracy.

Recently, Dos Santos et al. applied MetaD simulations to *closo*-hydride SSEs, demonstrating an exceptional match with experimental values for some complicated SSEs.[37] Based on the data summarized from previous reports, MetaD exhibits a high R^2 value of 0.95, which is proven to be a much more effective method, especially for those SSEs with large E_a (e.g., divalent SSEs). This direct benchmarking analysis shows that MetaD, due to its stronger capacity to map the global potential energy surface via applying a reasonable bias to the potential during simulations, could be a much more precise tool for the migration barrier prediction for SSEs.[38] In particular, this method shows a clear advantage in simulating divalent SSEs due to the relatively high migration barriers, which are difficult to overcome by conventional MD simulations.[37]

The above benchmarking analysis between experiments and theoretical computations based on LLM (Figure 1c) has subverted our previous understanding of some frequently used methods for transition-state searches in cation migration of SSEs. A significant discrepancy between conventional simulation methods and experimental E_a was revealed, indicating that more rational methods (e.g., MetaD) should be considered, especially for SSEs with higher E_a (e.g., divalent SSEs).

Next, we conduct a series of MetaD simulations to uncover the cation migration mechanisms within each SSE (Figure 1d). Alongside this, a variety of theoretical descriptors are introduced to describe the E_a of various SSEs, with the goal of discovering guiding principles for SSEs development. Finally, a global optimization strategy is employed to elucidate structures for the SSE compositions predicted with high ionic conductivity, verifying the potential candidates for SSEs. Throughout these steps, we integrate theoretical insights with experimental results to derive structure-property relationships, ultimately leading to the prediction of novel SSEs for battery applications. Overall, this workflow offers a powerful tool to predict the cation migration kinetics of hydrides and identify promising new candidates for SSEs.

Accurate Prediction and Novel Mechanisms of Cation Migration

To date, hydrides SSEs have been explored across various types of materials (Figure 2a). The cations predominantly include monovalent ions such as Li^+, Na^+, and K^+, as well as divalent ions such as Ca^{2+}, Mg^{2+}, and Zn^{2+}. The borohydride anions include smaller, *nido*-type ions (BH_4^-) and *arachno*-type ions ($B_3H_8^-$), along with the recently introduced "cage-like" *closo*-type ions (e.g., $B_nH_n^{x-}$ and $CB_nH_n^{x-}$). Neutral molecules such as H_2O, NH_3, NH_3BH_3, and CH_3NH_2 play a critical role in decreasing cation coordination and expanding the lattice, thereby enabling faster cation migration.[19,39,40] We systematically evaluated these cations and anions, including neutral molecules, through MetaD simulations for 21 different SSEs, with their free energy surfaces illustrated in Figures S1–S19 and migration processes illustrated in Supporting Movies. Figure 2b provides a comparison between the E_a obtained from MetaD simulations (labeled as MetaD E_a) and experiments (labeled as Experimental E_a; the experimental data and literature source are shown in Table S1), covering structures with (filled icons) and without (half-filled icons) neutral molecules. The MetaD E_a values were simulated at temperatures corresponding to the same phase observed in experiments. Excitingly, the E_a values derived from MetaD simulations show excellent agreement with experimental values (Figure 1b), boasting an R^2 value of 0.95. In particular, divalent SSEs with neutral molecules demonstrate outstanding benchmarking results, especially for those SSEs with higher E_a.

Besides, MetaD simulations help identify a novel cation migration process in SSEs, as illustrated by the Mg ion migration snapshots in Figure 2c. From 0 to 12 ps, the migrating Mg ion (highlighted in yellow) delocalizes from its original tetrahedral coordination, moves toward the neutral molecule (NH_3), and then shifts into the interstitial sites. During the 12–21 ps period, Mg ions continue their migration along the interstitials, alternately coordinating with the $[BH_4]^-$ anions to complete the migration. The profile of the spatial Mg-track (Figure 2d) indicates that the Mg-ion migrates -1.9 Å longitudinally and -1.0 Å vertically within 40 ps. Throughout
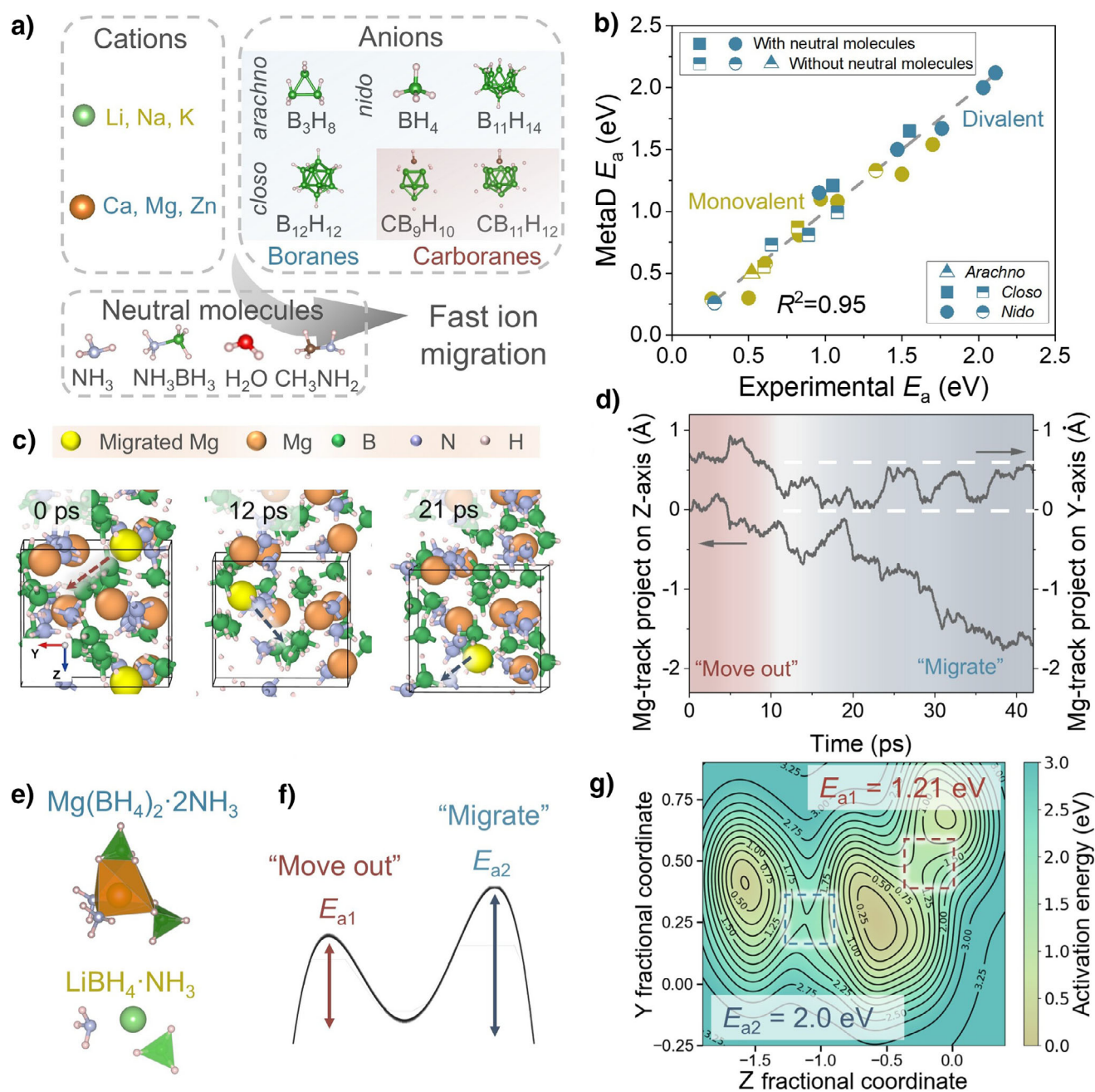
Figure 2. Experimental and simulated cation migration barriers of hydride SSEs. a) Typical cations, anions, and neutral molecules in hydride SSEs. b) Comparison between experimental E_a and the simulated E_a from MetaD simulations, for structures with (filled icons) and without (half-filled icons) neutral molecules. c) Snapshots of MetaD simulations of $Mg(BH_4)_2\cdot2NH_3$. d) The projected spatial track of Mg^{2+} ion (Mg-track project) during the simulations. e–f) The unit structure e) and migration process f) of $Mg(BH_4)_2\cdot2NH_3$ and $LiBH_4\cdot NH_3$. g) The potential energy surface of $Mg(BH_4)_2\cdot2NH_3$ captured by MetaD simulations.

this migration process, two quasi-stable Mg coordination states are observed. First, Mg^{2+} moves out from its original lattice position, a process resembling the "coordination-unlock" mechanism.[31] Second, the subsequent migration of Mg^{2+} is accompanied by the movement of $[BH_4]^-$ toward a nearby vacancy site, consistent with the "paddle-wheel" mechanism.[10] These two continuous processes last for 10 and 30 ps, respectively. Surprisingly, a similar cation migration process is also observed in $LiBH_4\cdot NH_3$ (Figure S20A). The

similar "moving out" process and the subsequent migration processes of Li^+ last for 10 and 8 ps, respectively. The spatial Li-track shows that it migrates -1.5 Å horizontally and -1.0 Å longitudinally within 18 ps.

When combining the unit structures of $Mg(BH_4)_2\cdot2NH_3$ and $LiBH_4\cdot NH_3$ (Figure 2e), cations are symmetrically surrounded by anions and neutral molecules. These SSEs exhibit two distinct E_a values: the first one, denoted as E_{a1}, corresponds to the cation moving out of its symmetrical

coordination environment; the second one (E_{a2}) relates to the subsequent migration of the cation to the vacancy nearby (Figure 2f). Figure 2g illustrates the potential energy surface of Mg-ion migration in $Mg(BH_4)_2 \cdot 2NH_3$. The two E_a values obtained from MetaD simulations are 1.21 eV for E_{a1} and 2.0 eV for E_{a2}. Combined with the Mg-track project (Figure 2d), E_{a1} represents the "moving out" process of Mg ion from its initial coordination site, while E_{a2} reflects the subsequent migration. Similarly, two E_a are also identified in $LiBH_4 \cdot NH_3$: 1.0 eV for the initial movement (E_{a1}), and 1.54 eV for the subsequent migration (E_{a2}) (Figure S20B–C). Interestingly, E_{a2} is higher than E_{a1}, suggesting that the subsequent migration step may be rate-determining, and more importantly, E_{a2} closely aligns with the experimentally measured E_a.[41]

Linear Correlation and General Trend of Divalent SSEs

MetaD has quantitatively captured the cation migration in divalent *closo*-type hydride SSEs, such as $MB_{12}H_{12} \cdot nH_2O$, where M represents Zn, Mg, and Ca, and n ranges from 2 to 12.[37] Building on this, we have expanded to include a broader series of hydrides, encompassing various cations, anions, and neutral molecules, specifically focusing on $Mg(BH_4)_2 \cdot nNH_3$, with $n = 0, 1, 2, 3$, and 6. To delve deeper into cation migration in hydrides and develop a general description for E_a, herein, eight theoretical descriptors are introduced: the volume of a unit cell per formula unit (V), Pauling electronegativity (X), atomic number of the system (Z), the binding energy of a moving cation (b_m), anion distance (d), number of the neutral molecules (n), atomic radius (r_{atom}), and ionic radius (r_{ion}). Single linear regressions comparing the *closo*- and *nido*-type systems reveal that *nido*-type system (i.e., the BH_4 system) generally exhibits higher R^2 values, indicating that SSEs with smaller anions demonstrate greater consistency in these regressions (Figure S21). For instance, for the BH_4 system, the correlation of E_a versus r_{atom}, X, and Z presents the R^2 of 0.99, 0.98, and 0.97, respectively. In contrast, the R^2 of these features are respectively 0.83, 0.86, and 0.78 for *closo*-SSEs. More excitingly, these three descriptors can be attributed as the intrinsic physical properties of the SSEs, requiring no additional ab initio computation, which makes them powerful descriptors for guiding the design of next-generation SSEs. Furthermore, to unify these two types of SSEs and extend our findings to a broader range of hydride SSEs, we explored multiple linear regressions using the equation $E_a = a_1 P_1 + a_2 P_2 + b$ (where P_i represents the selected properties, and a_i and b are the fitted parameters) (Figure 3a and Table S2). The best fit was achieved with both (r_{atom}, X) and (n, V), each yielding R^2 values of 0.91.

Figure 3b illustrates the multiple linear regression for divalent SSEs with neutral molecules, plotting E_a against (r_{atom}, X). The results from the MetaD simulations and experiments benchmarked with MetaD show a high level of conformity along the y_1 line, achieving an R^2 value of 0.91. These linear correlations align remarkably well with the available experimental data (Table S3) for divalent hydridoborate SSEs with neutral molecules (represented

by empty squares), underscoring their strong predictive capability in identifying novel hydride SSEs. The function ($x = -0.059 X + 0.0029 r_{atom}$) demonstrated along this line is then extended to other hydride SSEs. Another line, labeled as y_2, with an impressive R^2 of 0.98, includes results from the MetaD data of $Mg(CB_{11}H_{12})_2 \cdot 7.5H_2O$ and the experimental data of $M(CB_{11}H_{12})_2 \cdot nH_2O$ (M=Ca, Mg, and Zn) and $Mg(BH_4)_2 \cdot nCH_3NH_2$, where n ranges from 1 to 12. These two types of SSEs exhibit a distinct trend compared to boranes (line y_1), possibly due to the presence of carbon, which may induce the rotation of anions and neutral molecules. Interestingly, $Mg(BH_4)_2 \cdot nCH_3NH_2$ SSEs with $n = 1$ and $n = 6$ exhibit two phases, resulting in a lower E_a which follows the y_2 line.[29] While the one with only one phase (i.e., $Mg(BH_4)_2 \cdot 3CH_3NH_2$) exhibits a higher E_a, which follows the y_1 line. This suggests that when the neutral molecule contains carbon, the SSE may form multiple phases. This structural complexity could contribute to a potential reduction in E_a, consistent with the y_2 line.

Inspired by the remarkable conformity of the function ($x = -0.059 X + 0.0029 r_{atom}$) in neutral molecule-containing divalent hydride SSEs, we further extended the analysis to neutral molecule-containing monovalent SSEs (Figure S24). Encouragingly, the resulting line ($y = 0.89 x + 1.0$) shows a slope nearly identical to that of divalent SSEs (slope = 1.06, Figure 3b), suggesting that the E_a for neutral molecule-containing monovalent and divalent SSEs follow a universal trend with the independent variables X and r_{atom}. Due to the stronger electrostatic forces, divalent SSEs exhibit higher E_a, leading to a larger intercept.

Prediction and Validation of the High-Performance Divalent Hydride SSEs

Building on the two lines identified for divalent SSEs with neutral molecules (Figure 3b), two multiple linear correlation models are established to predict the behavior of a wide range of cations, anions, and neutral molecules, forming 558 potential SSEs (Figure 4a and Supporting Dataset). All SSEs in these models contain one of these cations: Ca^{2+}, Mg^{2+}, or Zn^{2+}, with the number of neutral molecules ranging from 0 to 6. The anions are boranes following line y_1, encompassing 270 potential SSEs. Meanwhile, the anions that are boranes and combine with carbon-containing neutral molecules, as well as the anions that are carboranes, follow line y_2, covering 108 and 180 potential SSEs, respectively. In both multiple linear correlation predictions, the SSEs with the lowest E_a are $M(BH_4)_2 \cdot 6(CH_3)_2CHNH_2$ (labeled as MBCCN, M=Ca, Mg, and Zn), with E_a values along line y_1 of 0.68 eV for CaBCCN, 0.57 eV for MgBCCN, and 0.51 eV for ZnBCCN. Considering the potential phase transition, these E_a values are even lower along line y_2, decreasing to 0.35, 0.32, and 0.31 eV, respectively. More excitingly, $Mg(BH_4)_2 \cdot 1.5(CH_3)_2CHNH_2$ has been experimentally synthesized with an activation energy of 1.22 eV which is consistent with line y_1.[42]

Given the limited information about these predicted SSEs, we introduced a crystal structure prediction method based on a genetic algorithm (GA) for global optimization, enabling us
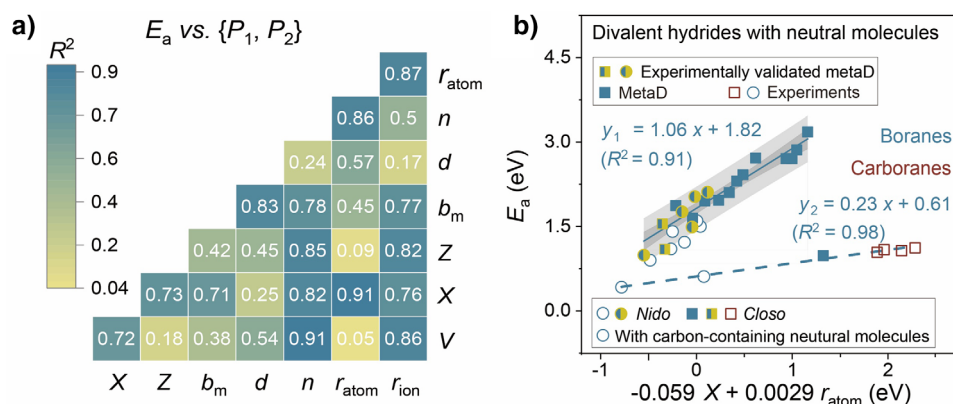
Figure 3. Correlation analysis between the migration E_a of hydride SSEs and theoretical descriptors. a) Feature analysis with the calculated coefficient of determination (R^2) for the considered eight properties against the E_a, including the volume of a unit cell per formula unit (V), Pauling electronegativity (X), atomic number of the system (Z), the binding energy of a moving cation (b_m), anion distance (d), number of the neutral molecules (n), atomic radius (r_{atom}), and ionic radius (r_{ion}). b) Multiple linear regressions for divalent SSEs with neutral molecules.
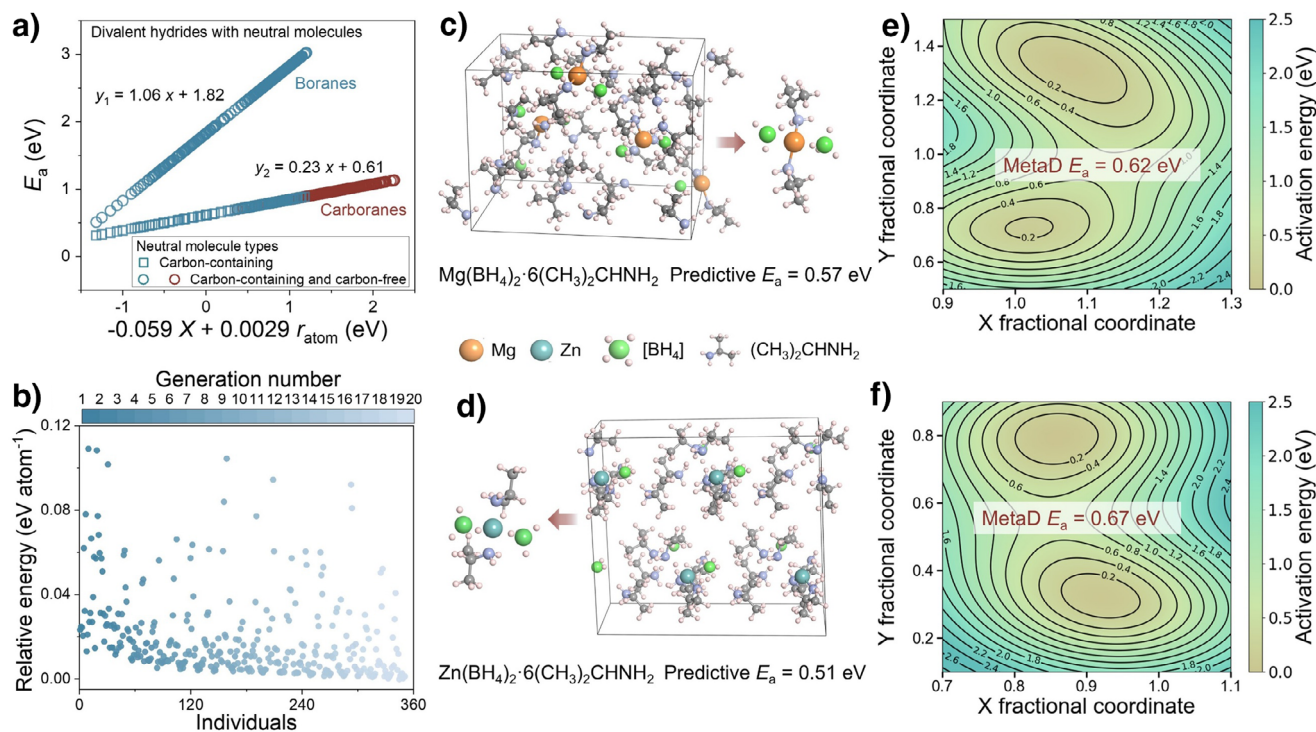
Figure 4. Prediction of hydride SSEs based on the workflow. a) Multiple linear correlation prediction of divalent hydride SSEs. b) Relative energy obtained along the generation. Global structures and local environments of c) $Mg(BH_4)_2 \cdot 6(CH_3)_2CHNH_2$ and d) $Zn(BH_4)_2 \cdot 6(CH_3)_2CHNH_2$. Potential energy surfaces of e) Mg-ion migration in $Mg(BH_4)_2 \cdot 6(CH_3)_2CHNH_2$ and f) Zn-ion migration in $Zn(BH_4)_2 \cdot 6(CH_3)_2CHNH_2$.

to uncover stable structures without relying on experimental data. This structure search strategy is crucial for neutral molecule-containing hydride SSEs due to the difficulty in identifying their highly complex structural information from current experimental techniques. First, the structures of $Mg(BH_4)_2 \cdot nNH_3$ (where $n = 0, 1, 2, 3$, and 6) were predicted using the USPEX package,[43] based on the SSEs' chemical compositions. In the coordination of hydrides, the cation forms a tetrahedral coordination with four $[BH_4]^-$ anions. When the neutral molecule is added, it replaces $[BH_4]^-$

and coordinates with the cation, facilitating the search for unknown structures using GA methods. Consequently, the structures of $Mg(BH_4)_2 \cdot nNH_3$ (where $n = 0, 1, 2, 3$, and 6) align well with experiments (Figures S25–S29).[19,44] Building on the success of GA in predicting the structures of $Mg(BH_4)_2 \cdot nNH_3$ SSEs, we applied this method to the three novel SSEs with the lowest E_a identified earlier (Figure 4a). Figures 4b, S30 and S31 illustrate the structural evolution of MBCCN across GA generations. Remarkably, the minimum energy structures were achieved after approximately 300

sampled individuals. Figures 4c,d and S30 present the globally optimized structures of MgBCCN and ZnBCCN, respectively, revealing that in both SSEs, the cations are coordinated with two $[BH_4]^-$ anions and two neutral molecules. Furthermore, the formation energy of CaBCCN, MgBCCN, and ZnBCCN are −0.006, −0.012, and −0.12 eV peratom, respectively, indicating stability of structure and demonstrating the high reliability of the GA method. To evaluate the accuracy of the linear relationship in Figure 4a, MetaD simulations were further conducted to investigate the E_a of both MgBCCN and ZnBCCN, along with the ion migration process depicted in Figure S32. In both cases, the Mg and Zn ions achieve migration by alternately coordinating with free neutral molecules within the lattice, resulting in E_a values of 0.62 and 0.67 eV, respectively (Figure 4e,f). When compared to the predicted E_a in Figure 4a, MgBCCN shows only a difference of 0.05 eV. This benchmarking analysis clearly demonstrates that this workflow effectively creates new possibilities to design and predict divalent hydride SSEs.

Conclusion

In this study, we developed a pioneering **data-driven AI framework** for discovering novel SSEs, integrating LLM, ab initio MetaD, multiple linear regression, GA, and theory-experiment benchmarking analysis. Our finding demonstrates that ab initio MetaD represents an optimal computational technique, achieving remarkable agreement with experimental data for complex hydride SSEs. Moreover, we identified a novel **"two-step" ion migration mechanism** in both monovalent and divalent hydride SSEs arising from the incorporation of molecular groups. Leveraging feature analysis combined with multiple linear regression, we successfully constructed precise **predictive models** for the rapid evaluation of hydride SSE performance. Notably, the proposed framework also enables accurate prediction of candidate structures **without relying on experimental inputs**. Collectively, this study provides transformative insights and advanced methodologies for the efficient design and optimization of next-generation SSBs, significantly contributing toward sustainable energy solutions.

Conflict of Interests

The authors declare no conflict of interest.

Data Availability Statement

The data that supports the findings of this study are included in the published article and its Supporting Materials. The experimental and computational data from literature and Supporting Movies are available in our Dynamic Database of Solid-State Electrolyte (DDSE: https://www.ddse-database.org/). The detailed introduction and insights of the large language model can be viewed in the Supporthing Video, which is available in our GitHub: https://github.com/qianwangfe/Data-Driven-Framework-for-Divalent-Electrolytes.git. In addition, all data in this work are available upon reasonable request from the corresponding author.

[1] N. Jones, *Nature* **2024**, *626*, 248–251.

[2] T. Famprikis, P. Canepa, J. A. Dawson, M. S. Islam, C. Masquelier, *Nat. Mater.* **2019**, *18*, 1278–1291.

[3] X. Yang, K. R. Adair, X. Gao, X. Sun, *Energy Environ Sci.* **2021**, *14*, 643–671.

[4] Q. Zhao, S. Stalin, C. Z. Zhao, L. A. Archer, *Nat. Rev. Mater.* **2020**, *5*, 229–252.

[5] J. Su, T. Tsuruoka, T. Tsujita, Y. Nishitani, K. Nakura, K. Terabe, *Chem. Mater.* **2019**, *31*, 5566–5575.

[6] P. Canepa, S.-H. Bo, G. Sai Gautam, B. Key, W. D. Richards, T. Shi, Y. Tian, Y. Wang, J. Li, G. Ceder, *Nat. Commun.* **2017**, *8*, 1759.

[7] R. Mohtadi, S. Orimo, *Nat. Rev. Mater.* **2016**, *2*, 16091.

[8] R. Mohtadi, M. Matsui, T. S. Arthur, S. Hwang, *Angew. Chem.* **2012**, *124*, 9918–9921.

[9] A. Manthiram, X. W. Yu, S. F. Wang, *Nat. Rev. Mater.* **2017**, *2*, 16103.

[10] Z. Zhang, L. F. Nazar, *Nat. Rev. Mater.* **2022**, *7*, 389–405.

[11] T. J. Udovic, M. Matsuo, A. Unemoto, N. Verdal, V. Stavila, A. V. Skripov, J. J. Rush, H. Takamura, S. Orimo, *Chem. Commun.* **2014**, *50*, 3750–3752.

[12] C. Yang, Q. Wu, W. Xie, X. Zhang, A. Brozena, J. Zheng, M. N. Garaga, B. H. Ko, Y. Mao, S. He, Y. Gao, P. Wang, M. Tyagi, F. Jiao, R. Briber, P. Albertus, C. Wang, S. Greenbaum, Y.-Y. Hu, A. Isogai, M. Winter, K. Xu, Y. Qi, L. Hu, *Nature* **2021**, *598*, 590–596.

[13] S. Kim, H. Oguchi, N. Toyama, T. Sato, S. Takagi, T. Otomo, D. Arunkumar, N. Kuwata, J. Kawamura, S. Orimo, *Nat. Commun.* **2019**, *10*, 1081.

[14] S. Körbe, P. J. Schreiber, *J. Michl, Chem. Rev.* **2006**, *106*, 5208–5249.

[15] M. Matsuo, Y. Nakamori, S. Orimo, H. Maekawa, H. Takamura, *Appl. Phys. Lett.* **2007**, *91*.

[16] Y. Liang, H. Dong, D. Aurbach, Y. Yao, *Nat. Energy* **2020**, *5*, 646–656.

[17] S. Hou, X. Ji, K. Gaskell, P. F. Wang, L. Wang, J. Xu, R. Sun, O. Borodin, C. Wang, *Science* **2021**, *374*, 172–178.

[18] M. Heere, A.-L. Hansen, S. Payandeh, N. Aslan, G. Gizer, M. H. Sørby, B. C. Hauback, C. Pistidda, M. Dornheim, W. Lohstroh, *Sci. Rep.* **2020**, *10*, 9080.

[19] Y. Yan, W. Dononelli, M. Jorgensen, J. B. Grinderslev, Y. S. Lee, Y. W. Cho, R. Cerny, B. Hammer, T. R. Jensen, *Phys. Chem. Chem. Phys.* **2020**, *22*, 9204–9209.

[20] G. Han, A. Vasylenko, L. M. Daniels, C. M. Collins, L. Corti, R. Chen, H. Niu, T. D. Manning, D. Antypov, M. S. Dyer, *Science* **2024**, *383*, 739–745.

[21] S. Zhang, F. Zhao, S. Wang, J. Liang, J. Wang, C. Wang, H. Zhang, K. Adair, W. Li, M. Li, *Adv. Energy Mater.* **2021**, *11*, 2100836.

[22] B. He, P. Mi, A. Ye, S. Chi, Y. Jiao, L. Zhang, B. Pu, Z. Zou, W. Zhang, M. Avdeev, S. Adams, J. Zhao, S. Shi, *Acta Mater.* **2021**, *203*, 116490.

[23] C. Cui, F. Bai, Y. Yang, Z. Hou, Z. Sun, T. Zhang, *Adv. Sci.* **2024**, *11*, 2310005.

[24] M. Palumbo, K. Kisu, V. Gulino, C. Nervi, L. Maschio, S. Casassa, S. Orimo, M. Baricco, *J. Phys. Chem. C* **2022**, *126*, 15118–15127.

[25] Y. Mo, S. P. Ong, G. Ceder, *Chem. Mater.* **2012**, *24*, 15–17.

[26] X. He, Y. Zhu, Y. Mo, *Nat. Commun.* **2017**, *8*, 15893.

[27] Z. Zheng, F. Florit, B. Jin, H. Wu, S. C. Li, K. Y. Nandiwale, C. A. Salazar, J. G. Mustakis, W. H. Green, K. F. Jensen, *Angew. Chem.* **2025**, *137*, e202418074.

[28] F. Yang, E. Campos dos Santos, X. Jia, R. Sato, K. Kisu, Y. Hashimoto, S. Orimo, H. Li, *Nano Mater. Sci.* **2024**, *6*, 256–262.

[29] M. B. Amdisen, J. B. Grinderslev, L. N. Skov, T. R. Jensen, *Chem. Mater.* **2023**, *35*, 1440–1448.

[30] Y. Yan, J. B. Grinderslev, Y.-S. Lee, M. Jørgensen, Y. W. Cho, R. Černý, T. R. Jensen, *Chem. Commun.* **2020**, *56*, 3971–3974.

[31] Q. Wang, H. Li, R. Zhang, Z. Liu, H. Deng, W. Cen, Y. Yan, Y. Chen, *Energy Storage Mater.* **2022**, *51*, 630–637.

[32] B. Singh, Y. Wang, J. Liu, J. D. Bazak, A. Shyamsunder, L. F. Nazar, *J. Am. Chem. Soc.* **2024**, *146*, 17158–17169.

[33] N. D. Lepley, N. A. W. Holzwarth, Y. A. Du, *Phys. Rev. B* **2013**, *88*, 104103.

[34] K. Homma, M. Yonemura, T. Kobayashi, M. Nagao, M. Hirayama, R. Kanno, *Solid State Ionics* **2011**, *182*, 53–58.

[35] M. Tachez, J.-P. Malugani, R. Mercier, G. Robert, *Solid State Ionics* **1984**, *14*, 181–185.

[36] Q. Wang, J.-F. Wu, Z. Lu, F. Ciucci, W. K. Pang, X. Guo, *Adv. Funct. Mater.* **2019**, *29*, 1904232.

[37] E. Campos dos Santos, R. Sato, K. Kisu, K. Sau, X. Jia, F. Yang, S. Orimo, H. Li, *Chem. Mater.* **2023**, *35*, 5996–6004.

[38] K. Meier, T. Laino, A. Curioni, *J. Phys. Chem. C* **2014**, *118*, 6668–6679.

[39] K. Kisu, A. Dorai, S. Kim, R. Hamada, A. Kumatani, Y. Horiguchi, R. Sato, K. Sau, S. Takagi, S. Orimo, *J. Mater. Chem. A* **2022**, *10*, 24877–24887.

[40] K. Kisu, S. Kim, M. Inukai, H. Oguchi, S. Takagi, S. Orimo, *Acs Appl. Energ Mater.* **2020**, *3*, 3174–3179.

[41] T. Zhang, Y. Wang, T. Song, H. Miyaoka, K. Shinzato, H. Miyaoka, T. Ichikawa, S. Shi, X. Zhang, S. Isobe, N. Hashimoto, Y. Kojima, *Joule* **2018**, *2*, 1522–1533.

[42] L. G. Kristensen, M. B. Amdisen, L. N. Skov, T. R. Jensen, *Phys. Chem. Chem. Phys.* **2022**, *24*, 18185–18197.

[43] A. O. Lyakhov, A. R. Oganov, H. T. Stokes, Q. Zhu, *Comput. Phys. Commun.* **2013**, *184*, 1172–1182.

[44] X. Zhou, A. R. Oganov, G. Qian, Q. Zhu, *Phys. Rev. Lett.* **2012**, *109*, 245503.